Structural, Magnetic, and Ion-Exchange Properties of a New Layered Alkaline/Alkaline Earth Iron Phosphate: $NaBaFe_4(HPO_4)_3(PO_4)_3 \cdot H_2O$

Michael B. Korzenski and Joseph W. Kolis*

Department of Chemistry, Clemson University, Clemson, South Carolina 29634-0973

Received February 14, 2000

A new mixed alkali/alkaline earth iron phosphate, $NaBaFe_4(HPO_4)_3(PO_4)_3 \cdot H_2O$, has been synthesized hydrothermally and structurally characterized by single-crystal X-ray diffraction, magnetic susceptibility, infrared spectroscopy, and thermogravimetric analysis. The title compound crystallizes in the monoclinic space group $P2_1/c$ (No. 14) with $a = 9.287(2)$ Å, $b = 22.665(4)$ Å, $c = 8.966(3)$ Å, $\beta = 91.82(2)$, and $Z = 4$. The compound has a 2-D framework structure constructed from layers, stacked along the [010] unit cell direction with Na^+ and Ba^{2+} ions, and water molecules residing within the interlayer space. The anionic layers are composed from the assemblage of vertex shared FeO_6 octahedra interconnected by PO_4^{3-} and HPO_4^{2-} tetrahedra. The layers are built from four unique FeO_6 units linking through vertex shared oxygen atoms to form infinite zigzag chains that run parallel to the *a* axis. These chains form single layers that run infinitely in the *c* direction through the vertex sharing of PO_4 groups.

Introduction

Microporous solids, which incorporate transition metal atoms into the inorganic framework, may possess novel catalytic, magnetic, and ion-exchange properties, as well as high ionic conductivity, for potential fuel cell applications.[1−6] An extensive series of alkali metal cobalt phosphates which display many micorporous properties have been prepared recently at relatively low temperatures (<200 °C) using hydrothermal techniques.[7] We are exploring the synthesis of alkali and alkaline earth iron metal phosphates using hydrothermal reactions at relatively high temperatures (>350 °C). Our attention is focused on iron due to its ability to form solids with complex octahedral−tetrahedral frameworks of edge- and vertex-sharing MO_6 units, which possess interesting magnetic catalytic and/or electronic properties. [9,10] Among other things, we have found that the nature of the products of these hydrothermal reactions is extremely sensitive to the reaction conditions and a wide variety of new materials have been prepared. As a part of our ongoing research, we have extended our search of new inorganic framework materials by using combinations of group IA and group IIA metal cations as structure-directing agents. To our knowledge there has been only one previous report of a pure, well-characterized group IA/IIA iron phosphate, namely, $KBaFe_2(PO_4)_2$ which has the three-dimensional langbeinite structure.[11] By taking advantage of differences in size and coordination geometry of the group IA and group IIA metals, we have isolated the layered compound, $NaBaFe_4(HPO_4)_3(PO_4)_3 \cdot H_2O$, which exhibits a completely new structure type. Layered compounds are significant in that they can be used for ion-exchange or -storage applications.[12] In this paper we report the synthesis, crystal structure determination, magnetic properties, and ion-exchange potential of an unusual iron phosphate containing both an alkali and alkaline-earth metal cations.

Experimental Section

General. All reagents were of analytical grade and used as purchased from Aldrich Chemical Co. Qualitative elemental analysis on single-crystal samples of the title compound was obtained by energy dispersive spectrometry (EDS) using a JEOL JSM-IC 848 scanning microscope equipped with a Princeton Gamma Tech (PGT) PRISM detector and indicated the presence of Na, Ba, Fe, and P with no significant impurity heavier than F. Thermogravimetric analyses were performed on a DuPont Instruments 951 analyzer, while differential thermal analyses were performed using a DuPont Instruments Thermal Analyst 2000 equipped with a high-temperature 1600 DTA cell adapter. The samples were heated at 5° min^{-1} from 30 to 1100 °C, isothermed for 5 min, and then cooled to the starting temperature at the same rate in an atmosphere of oxygen. The infrared absorption spectra of KBr pellets were studied in the range of 400−4000 cm^{-1} using a Nicolet Magna-IR Spectrometer 550 with a Spectra Tech IR−Plan Laboratory Microscope single-crystal attachment.

Synthesis of $NaBaFe_4(HPO_4)_3(PO_4)_3 \cdot H_2O$. Single crystals of the title compound were prepared from a reaction mixture consisting of 0.0155 g (0.39 mmol) NaOH, 0.09 g (0.39 mmol) $BaHPO_4$, and 0.09 g (0.39 mmol) Fe_3O_4 (molar ratio of Na:Ba:Fe = 1:1:3), 0.1 mL of 85% H_3PO_4, and 0.5 mL of distilled water. The reaction mixture was

* To whom correspondence should be addressed. Telephone: 864-656-4739. Fax: 864-656-6613. E-mail: KJOSEPH@CLEMSON.EDU.

(1) Papoutsakis, D.; Jackson, J. E.; Nocera, D. G. *Inorg. Chem.* **1996**, *35*, 800.
(2) Casan, N.; Amoros, P.; Ibanez, R.; Martinez, E.; Beltran-Porter, A.; Beltran-Porter, D. *J. Inclusion Phenom.* **1988**, *6*, 193.
(3) Beltran-Porter, D.; Amoros, P.; Ibanez, R.; Le Bail, A.; Ferey, G.; Villeneuve, G. *Solid State Ionics* **1989**, *32*, 57.
(4) Beltran-Porter, D.; Beltran-Porter, A.; Amoros, P.; Ibanez, R.; Martinez, E.; Le Bail, A.; Ferey, G.; Villeneuve, G. *Eur. J. Solid State Inorg. Chem.* **1991**, *28*, 131.
(5) Brochu, R.; Lamzibri, A.; Aadane, A.; Arsalane, S.; Ziyad, M. *Eur. J. Solid State Inorg. Chem.* **1991**, *28*, 253.
(6) Clearfield, A. *Eur. J. Solid State Inorg. Chem.* **1991**, *28*, 37.
(7) Feng, P.; Bu, X.; Tolbert, S. H.; Stucky, G. D. *J. Am. Chem. Soc.* **1997**, *119*, 2497.
(8) Feng, P.; Bu, X.; Stucky, G. D. *Nature* **1997**, *388*, 735.
(9) Korzenski, M. B.; Schimek, G. L.; Kolis, J. W.; Long, G. J. *J. Solid State Chem.* **1998**, *139*, 152.
(10) Korzenski, M. B.; Kolis, J. W.; Long, G. J *J. Solid State Chem.* **1999**, *147*, 390.
(11) Battle, P. D.; Cheetham, A. K.; Harrison, W. T. A.; Long, G. J. *J. Solid State Chem.* **1986**, *62*, 16.
(12) Clearfield, A. *Chem. Rev.* **1988**, *88*, 125.

10.1021/ic0001513 CCC: $19.00
Published on Web 11/22/2000

sealed inside an evacuated quartz ampule, placed inside a Parr reaction autoclave, which was subsequently counterpressured with 3000 psi of argon. The autoclave was then heated at 375 °C for 3 days followed by cooling under a flow of nitrogen gas for approximately 30 min. The products were filtered and washed with water and acetone repeatedly and dried in an oven at 62 °C for 1 h. The products consisted of a mixture of tan tabular column crystals and green diamonds, each in approximately 50% yields, and were easily separated with the aid of ultrasonification. The X-ray powder pattern of a powdered sample of the tan crystals agreed well with that calculated from single-crystal data. The green diamonds were later confirmed to be another new phase, $Ba_2Fe_5(PO_4)_6 \cdot H_2O$, which will be discussed in detail elsewhere.[13] Attempts were made to prepare the potassium and rubidium analogues of the title compound by duplicating the above reaction and substituting NaOH with either KOH or RbOH. Both reaction products consisted of brown platelike crystals in very low yields. However, due to the severe twinning nature of the crystals, single-crystal X-ray data were never obtained.

Ion-Exchange Studies. Approximately 50 mg of $NaBaFe_4(HPO_4)_3(PO_4)_3 \cdot H_2O$ was added to a supersaturated solution of the corresponding MCl or MNO_3 salt (where M = Li^+, K^+, and Rb^+) in a 50 mL round-bottom flask. The aqueous solution was refluxed for 48 h, filtered, and then washed repeatedly with copious amounts of deionized water and acetone. The powdered sample was then dried in an oven at 60 °C for 2 h. Powder XRDs of the samples were run at the same continuous scan speeds as $NaBaFe_4(HPO_4)_3(PO_4)_3 \cdot H_2O$.

Single-Crystal X-ray Diffraction. A single-crystal having dimensions of 0.19 × 0.12 × 0.10 mm^3 was mounted on a glass fiber with a minimal amount of epoxy glue, for indexing and intensity data collection on a Rigaku AFC7R four-circle diffractometer equipped with graphite monochromated Mo Ka radiation (λ = 0.710 73 Å). The final unit cell parameters and orientation matrix were determined by a least-squares fit of 25 randomly located reflections between 39.85 and 54.72 in 2θ. Data were collected on a monoclinic cell using a $\theta-2\theta$ scan mode at 12°/min with up to 6 rescans to a maximum 2θ of 55° for the $\pm h, -k, +l$ quadrant. A total of 4713 reflections were collected of which 4320 were unique and 3557 were observed. The data were corrected for Lorentz and polarization effects, and an empirical correction based on ψ-scans[14] for three reflections with χ angles close to 90° was applied to compensate for absorption effects. Intensities of three check reflections monitored every 100 reflections remained invariant, indicating no sign of crystal decay.

On the basis of lattice parameters, Laue symmetry tests, the reflection conditions $h0l$ ($l = 2n$) and $0k0$ ($k = 2n$), and the subsequent successful structural refinement, the centrosymmetric space group $P2_1/c$ (No. 14) was uniquely determined. Also, the space group determination was confirmed via the MISSYM[15] algorithm within the PLATON[16] program suite. Structure determination and refinement were performed on a Digital VAXstation 4000 using the SHELXTL-PLUS program packages.[17] The structure was solved by direct methods using SHELXS-86,[18] and refined using full-matrix least-squares techniques with scattering factors taken from the source programs. The positions of the metal and phosphorus atoms were located initially, and the oxygen atoms were found in difference Fourier maps. Hydrogen atoms were fixed. All other atomic thermal parameters were refined anisotropically. The effects of secondary extinction were considered in the least squares refinement for low ordered data ($F_{obs} < F_{cal}$). The crystallographic data for $NaBaFe_4(HPO_4)_3(PO_4)_3 \cdot H_2O$ are listed in Table 1, while the atomic coordinates and the bond distances and bond valence sums are given in Tables 2 and 3, respectively.

(13) Korzenski, M. B.; Kolis, J. W.; Long, G. To be submitted for publication.
(14) North, A. C. T.; Phillips, D. C.; Mathews, F. S. *Acta Crystallogr.* **1968**, *A24*, 351.
(15) Spek, A. L. *Acta Crystallogr.* **1990**, *A46*, 334.
(16) Lepage, Y. *J. Appl. Crystallogr.* **1987**, *20*, 264.
(17) Sheldrick, G. M. *SHELXTL-PLUS Crystallographic System*, Release 4.11; Siemens Analytical X-ray Instruments Inc.: Madison, WI, 1990.
(18) Sheldrick, G. M. SHELXS-86. In *Crystallographic Computing 3*; Sheldrick, G. M., Kroger, C., Goddard, R., Eds.; Oxford University Press: London/New York, 1985; pp 175−189.

Table 1. Crystallographic Data and Structure Refinement for $NaBaFe_4(HPO_4)_3(PO_4)_3 \cdot H_2O$

empirical formula	$NaBaFe_4P_6O_{25}H_3$
formula wt (g/mol)	972.6
space group, Z	$P2_1/c$, 4
a (Å)	9.287(2)
b (Å)	22.665(4)
c (Å)	8.966(3)
β (deg)	91.82(2)
V ($Å_3$)	1886.3(8)
d_{calc} (g cm^{-3})	3.425
λ (Mo Ka, Å)	0.710 74
T (°C)	20
μ (mm^{-1})	5.726
R,[a] R_w[b]	0.0346, 0.0469

[a] $R = \sum||F_o| - |F_c||/\sum|F_o||$. [b] $R_w = [\sum w\{|F_o| - |F_c|\}^2/\sum w|F_o|^2]^{1/2}$; $w = 1/[\sigma^2(F) + 0.0005F^2]$.

Table 2. Atomic Coordinates and Thermal Parameters[a] for $NaBaFe_4(HPO_4)_3(PO_4)_3 \cdot H_2O$

atom	x	y	z	U_{eq}
Ba(1)	0.3438(3)	0.4163(1)	0.4647(3)	0.19(1)
Na(1)	0.2881(3)	0.1081(1)	0.3834(3)	0.35(7)
Fe(1)	0.8336(6)	0.2888(3)	0.2159(7)	0.14(2)
Fe(2)	0.1668(6)	0.3752(3)	0.4125(7)	0.14(2)
Fe(3)	0.3371(6)	0.1244(3)	0.4659(7)	0.14(2)
Fe(4)	0.5813(7)	0.2918(3)	0.7083(7)	0.14(2)
P(1)	0.8322(1)	0.2481(5)	0.4614(1)	0.13(3)
P(2)	0.3327(1)	0.2457(5)	0.4628(1)	0.13(3)
P(3)	0.8860(1)	0.1415(5)	0.2103(1)	0.14(3)
P(4)	0.8381(1)	0.4303(5)	0.1503(1)	0.13(3)
P(5)	0.5841(1)	0.3562(5)	0.2140(1)	0.14(3)
P(6)	0.5766(1)	0.6502(5)	0.2705(1)	0.13(3)
O(1)	0.829(3)	0.2976(1)	0.6113(4)	0.16(9)
O(2)	0.2507(4)	0.2853(1)	0.3539(4)	0.19(10)
O(3)	0.2306(3)	0.2996(1)	0.3865(4)	0.15(9)
O(4)	0.6673(3)	0.2860(1)	0.3727(4)	0.16(9)
O(5)	0.8347(4)	0.2065(2)	0.1799(4)	0.23(10)
O(6)	0.9621(4)	0.3746(2)	0.2438(4)	0.18(9)
O(7)	0.6900(4)	0.3830(2)	0.1099(4)	0.21(1)
O(8)	0.2419(4)	0.3792(2)	0.1863(4)	0.25(1)
O(9)	0.6443(3)	0.4367(2)	0.810(4)	0.17(9)
O(10)	0.7447(3)	0.29840(2)	0.8659(4)	0.17(9)
O(11)	0.7282(3)	0.6171(2)	0.3453(4)	0.17(9)
O(12)	0.7327(3)	0.2888(1)	0.5454(4)	0.17(9)
O(13)	0.4368(3)	0.2994(1)	0.8891(4)	0.15(9)
O(14)	0.4139(3)	0.2864(2)	0.5693(47)	0.17(9)
O(15)	0.2368(3)	0.3807(2)	0.7593(4)	0.18(9)
O(16)	0.4328(3)	0.3778(2)	0.1748(4)	0.17(9)
O(17)	0.4676(3)	0.6497(2)	0.3627(4)	0.17(9)
O(19)	0.5778(4)	0.3888(2)	0.5521(4)	0.21(10)
O(20)	0.1081(4)	0.4813(2)	0.6855(4)	0.16(9)
O(22)	0.5963(4)	0.2909(2)	0.2307(4)	0.22(10)
O(23)	0.6211(4)	0.3820(2)	0.3761(4)	0.19(10)
O(24)	0.4528(4)	0.5149(2)	0.3356(4)	0.20(10)
O(25)	0.2066(4)	0.5104(2)	0.6176(5)	0.35(10)
H(1)	0.1733	0.5200	0.2205	0.080
H(2)	0.6652	0.3547	0.4305	0.080
H(3)	0.0003	0.3691	0.4876	0.080

[a] The equivalent isotropic temperature factor, U_{eq}, is defined as $^1/_3\{\Sigma_i\Sigma_j(U_{ij}a^*_i a^*_j a_i a_j)\}$, where the summations of i and j range from 1 to 3.

Results and Discussion

Crystal Structure. The structure of $NaBaFe_4(HPO_4)_3(PO_4)_3 \cdot H_2O$ exhibits a new structure type consisting of a layered framework composed of vertex-shared FeO_6 octahedra connected by PO_4 and HPO_4 tetrahedra. (Figure 1). The basic building block of each layer consists of zigzag chains of FeO_6 octahedra connected via vertex sharing, which run parallel to the a axis. These chains are interconnected into single layers that run infinitely in the c direction through the vertex sharing

Table 3. Selected Bond Distances (Å) and Angles (deg) with ESD's for $NaBaFe_4(HPO_4)_3(PO_4)_3 \cdot H_2O$

Bond Distances (Å)

Fe(1)−O(1)	2.053(3)	Fe(1)−O(2)	1.957(3)	P(4)−O(6)	1.516(4)	P(4)−O(9)	1.510(3)
Fe(1)−O(3)	2.143(3)	Fe(1)−O(4)	2.012(3)	P(4)−O(18)	1.522(3)	P(4)−O(20)	1.574(3)
Fe(1)−O(5)	1.892(4)	Fe(1)−O(6)	1.966(3)	P(5)−O(7)	1.505(4)	P(5)−O(16)	1.518(3)
Fe(2)−O(1)	2.121(3)	Fe(2)−O(7)	1.936(4)	P(5)−O(22)	1.493(4)	P(5)−O(23)	1.595(3)
Fe(2)−O(8)	1.888(4)	Fe(2)−O(9)	1.981(3)	P(6)−O(11)	1.542(3)	P(6)−O(17)	1.546(3)
Fe(2)−O(10)	2.088(3)	Fe(2)−O(11)	1.991(3)	P(6)−O(21e)	1.542(3)	P(6)−O(24)	1.501(4)
Fe(3)−O(3)	2.101(3)	Fe(3)−O(13)	2.088(3)	Na(1)−O(17)	2.394(4)	Na(1)−O(7)	2.416(4)
Fe(3)−O(15)	2.050(3)	Fe(3)−O(16)	2.049(3)	Na(1)−O(9)	2.428(4)	Na(1)−O(11)	2.700(4)
Fe(3)−O(17)	1.925(3)	Fe(3)−O(18)	1.947(3)	Na(1)−O(18)	2.371(4)	Na(1)−O(25)	2.478(5)
Fe(4)−O(10)	2.046(3)	Fe(4)−O(12)	2.060(3)	Ba(1)−O(2)	3.239(4)	Ba(1)−O(6)	3.132(3)
Fe(4)−O(13)	2.144(3)	Fe(4)−O(14)	1.965(3)	Ba(1)−O(14)	3.150(3)	Ba(1)−O(15)	2.964(3)
Fe(4)−O(21)	1.926(3)	Fe(4)−O(22)	1.888(4)	Ba(1)−O(16)	2.887(3)	Ba(1)−O(19)	2.862(4)
P(1)−O(12)	1.522(3)	P(1)−O(1)	1.565(3)	Ba(1)−O(20)	3.138(3)	Ba(1)−O(21)	2.945(3)
P(1)−O(4)	1.516(3)	P(1)−O(10)	1.568(3)	Ba(1)−O(23)	2.828(3)	Ba(1)−O(24)	2.727(3)
P(2)−O(2)	1.513(4)	P(2)−O(14)	1.513(3)	Ba(1)−O(25)	2.857(4)	Ba(1)−O(24)	2.999(3)
P(2)−O(3)	1.567(3)	P(2)−O(13)	1.566(3)	O(11)−H(1)	1.454(3)	O(19)−H(3)	0.897
P(3)−O(5)	1.500(4)	P(3)−O(8)	1.496(4)	O(20)−H(1)	1.153	O(23)−H(2)	0.881
P(3)−O(15)	1.516(3)	P(3)−O(19)	1.593(4)				

Bond Angles (deg)

O(1)−Fe(1)−O(2)	175.2(1)	O(1)−Fe(1)−O(3)	88.4(1)	O(12)−Fe(4)−O(13)	175.0(1)	O(12)−Fe(4)−O(14)	95.3(1)
O(1)−Fe(1)−O(4)	87.3(1)	O(1)−Fe(1)−O(5)	89.2(1)	O(12)−Fe(4)−O(21)	90.9(1)	O(12)−Fe(4)−O(22d)	89.6(1)
O(1)−Fe(1)−O(6)	91.7(1)	O(2)−Fe(1)−O(3)	87.8(1)	O(13)−Fe(4)−O(14)	89.0(1)	O(13)−Fe(4)−O(21)	87.0(1)
O(2)−Fe(1)−O(4)	96.4(1)	O(2)−Fe(1)−O(5)	93.7(1)	O(13)−Fe(4)−O(22A)	92.6(1)	O(14)−Fe(4)−O(21)	86.0(1)
O(2)−Fe(1)−O(6)	85.2(1)	O(3)−Fe(1)−O(4)	173.8(1)	O(14)−Fe(4)−O(22A)	93.5(1)	O(21)−Fe(4)−O(22A)	179.4(1)
O(3)−Fe(1)−O(5)	89.0(1)	O(3)−Fe(1)−O(6)	86.7(1)	O(1f)−P(1)−O(10e)	96.3(2)	O(1f)−P(1)−O(4 g)	111.5(2)
O(4)−Fe(1)−O(5)	95.3(1)	O(4)−Fe(1)−O(6)	89.0(1)	O(4 g)−P(1)−O(10e)	114.4(2)	O(12)−P(1)−O(1f)	114.9(2)
O(5)−Fe(1)−O(6)	175.6(2)	O(1)−Fe(2)−O(7b)	91.4(1)	O(12)−P(1)−O(4 g)	108.2(2)	O(12)−P(1)−O(10e)	111.4(2)
O(1)−Fe(2)−O(8)	94.7(1)	O(1)−Fe(2)−O(9)	100.7(1)	O(2)−P(2)−O(3d)	111.7(2)	O(2)−P(2)−O(13e)	114.8(2)
O(1)−Fe(2)−O(10b)	67.4(1)	O(1)−Fe(2)−O(11c)	169.6(1)	O(2)−P(2)−O(14)	106.0(2)	O(3d)−P(2)−O(13e)	98.4(2)
O(7b)−Fe(2)−O(10b)	94.8(1)	O(7b)−Fe(2)−O(11c)	87.5(1)	O(14)−P(2)−O(3d)	115.0(2)	O(14)−P(2)−O(13e)	111.2(2)
O(8)−Fe(2)−O(7b)	172.0(2)	O(8)−Fe(2)−O(9)	90.2(1)	O(5)−P(3)−O(8d)	113.7(2)	O(5)−P(3)−O(15e)	113.6(2)
O(8)−Fe(2)−O(10b)	92.4(1)	O(8)−Fe(2)−O(11c)	87.5(1)	O(5)−P(3)−O(19e)	104.9(2)	O(8d)−P(3)−O(15e)	111.3(2)
O(9)−Fe(2)−O(7b)	83.5(1)	O(9)−Fe(2)−O(10b)	168.0(1)	O(8d)−P(3)−O(19e)	107.9(2)	O(15e)−P(3)−O(19e)	104.6(2)
O(9)−Fe(2)−O(11c)	89.4(1)	O(10b)−Fe(2)−O(11c)	102.4(1)	O(6)−P(4)−O(9)	111.7(2)	O(6)−P(4)−O(18)	112.0(2)
O(3d)−Fe(3)−O(13e)	69.0(1)	O(3d)−Fe(3)−O(15e)	97.0(1)	O(6)−P(4)−O(20)	103.6(2)	O(9)−P(4)−O(18)	111.7(2)
O(3d)−Fe(3)−O(16d)	86.0(1)	O(13e)−Fe(3)−O(15e)	86.7(1)	O(9)−P(4)−O(20)	108.9(2)	O(18)−P(4)-O(20)	108.4(2)
O(13e)−Fe(3)−O(16d)	97.9(1)	O(13e)−Fe(3)−O(18d)	165.5(1)	O(7)−P(5)−O(16)	110.2(2)	O(7)−P(5)−O(22)	114.4(2)
O(15e)−Fe(3)−O(16d)	175.2(1)	O(17)−Fe(3)−O(3d)	168.5(1)	O(7)−P(5)−O(23)	106.9(2)	O(16)−P(5)−O(22)	114.2(2)
O(17)−Fe(3)−O(13e)	100.6(1)	O(17)−Fe(3)−O(16d)	90.9(1)	O(16)−P(5)−O(23)	105.3(2)	O(22)−P(5)−O(23)	105.0(2)
O(17)−Fe(3)−O(15e)	86.8(1)	O(10)−Fe(4)−O(12)	89.1(1)	O(11)−P(6)−O(17)	106.9(2)	O(11)−P(6)−O(21e)	108.2(2)
O(10)−Fe(4)−O(13)	86.6(1)	O(10)−Fe(4)−O(14)	175.6(1)	O(11)−P(6)−O(24h)	112.6(2)	O(17)−P(6)−O(21e)	108.8(2)
O(10)−Fe(4)−O(21)	93.4(1)	O(10)−Fe(4)−O(22d)	87.1(1)	O(17)−P(6)−O(24h)	110.8(2)	O(21e)−P(6)−O(24h)	109.5(2)

of bridging phosphate groups (Figure 2). The layers are stacked along the [010] unit cell direction with the sodium and barium ions and the water molecule located between the layers. All four crystallographically unique iron atoms are coordinated to six oxygen atoms and are formally trivalent, as indicated by bond valence calculations (Table 4). All four FeO_6 octahedra are slightly distorted with average Fe−O distances of 2.00(9), 2.00(9), 2.03(7), and 2.00(9) Å for Fe(1), Fe(2), Fe(3), and Fe(4), respectively. The calculated degrees of distortion are 9.5, 9.9, 6.6, and 11 ($\Delta = 10^3$), for Fe(1), Fe(2), Fe(3), and Fe(4), respectively. [19]

There are six unique phosphorus atoms, P(1), P(2), and P(6) which form PO_4^{3-} groups, while P(3), P(4), and P(5) are assigned as HPO_4^{2-} groups. The PO_4 groups all adopt the expected tetrahedral geometry and possess average P−O distances of 1.54(4) Å which correlate well with the expected value predicted by Shannon.[19] However, P(3), P(4), and P(5) which form the HPO_4^{2-} groups possess longer P−O distances (P(3)−O(19) = 1.593(4) Å, P(4)−O(20) = 1.574(3) Å, and P(5)−O(23) = 1.595(3) Å), which are typical for OH groups in HPO_4^{2-} molecules.[20−23] Note also the low bond valence sums for O(19), O(20), and O(23), respectively (Table 4). The $P(1)O_4$ and $P(2)O_4$ are both edge and vertex sharing to FeO_6 octahedra, while $HP(3)O_4$, $HP(4)O_4$, $HP(5)O_4$, and $P(6)O_4$ are only vertex shared to FeO_6 octahedra. The $P(1)O_4$ and $P(2)O_4$ are not responsible for stitching the FeO_6 chains together, but they do serve to link the individual chains together in the *c* direction. The four remaining phosphate and hydrogen phosphate groups link the chains together in the *a* direction and possess a terminal P−O bond that points inward toward the small cavities formed by the zigzag nature of the layers (Figure 3). With the exception of O(24), the remaining oxygen atoms of these P−O bonds are subsequently attached to a hydrogen atom.

The barium cations occupy pockets created by the corrugated nature of the layers and are coordinated by 12 oxygen atoms. Three of the oxygen atoms are terminal atoms on the three HPO_4^{2-} groups, while eight oxygen atoms are vertex shared with FeO_6 or PO_4 groups. The remaining oxygen atom O(25) belongs to the water molecule and is the only link between the barium and sodium cations. The sodium cations reside between the interlayer spaces and are coordinated to six oxygen atoms, all of which are vertex shared to FeO_6 and PO_4 groups.

(19) Shannon, R. D. *Acta Crystallogr*. **1976**, *A32*, 751.
(20) Lightfoot, P.; Cheetham, A. K.; Sleight, A. W. *J. Solid State Chem*. **1988**, *73*, 325.
(21) Lii, K.-H.; Shih, P.-F. *Inorg. Chem*. **1994**, *33*, 3028.
(22) Vencato, I.; de Farias, M. L.; Mattievich, E.; Primerano, M. Y. *J. Braz. Chem. Soc*. **1994**, *5*, 43.
(23) Lu, Y.; Haushalter, R. C.; Zubieta, J. *Inorg. Chim. Acta* **1998**, *268*, 257.

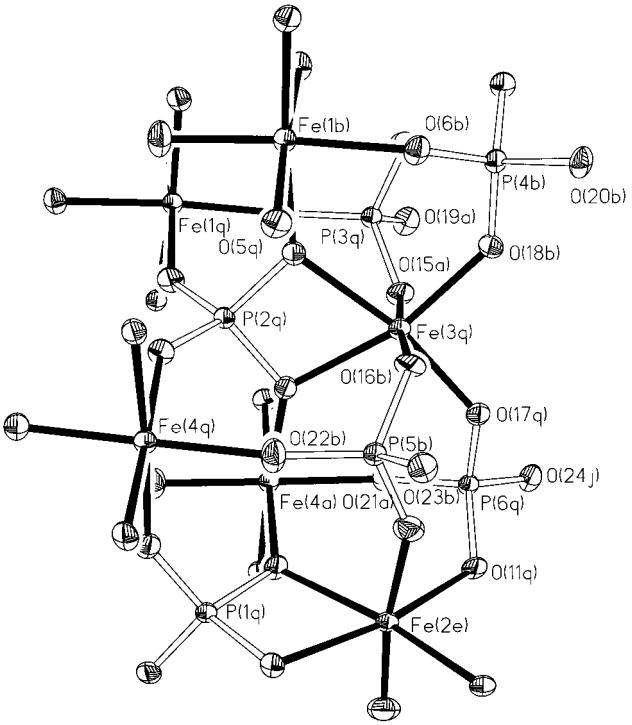

Figure 1. Unit cell view of the layers in $NaBaFe_4(HPO_4)_3(PO_4)_3 \cdot H_2O$ stacked along the (010) unit cell direction. The barium atoms are represented as crosshatched spheres, sodium atoms as lined spheres, the water molecule as an open sphere, the FeO_6 octahedra as lined structures, and the PO_4 tetrahedra as dotted structures.

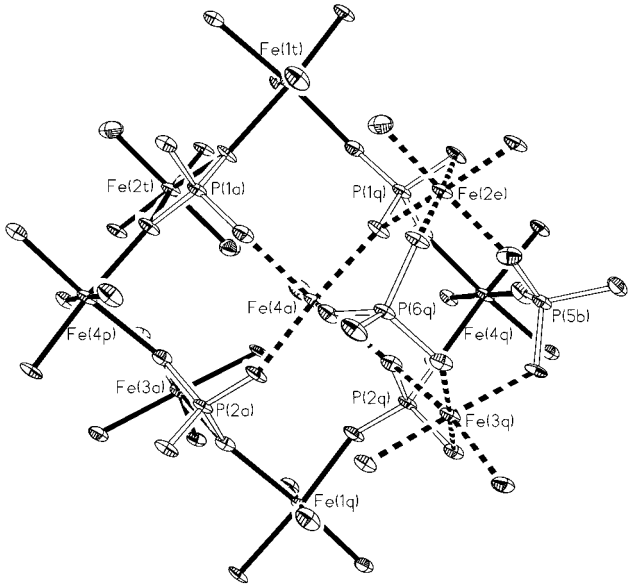

Figure 2. Section of the layer in $NaBaFe_4(HPO_4)_3(PO_4)_3 \cdot H_2O$ constructed from the four FeO_6 octahedra linking through vertex shared oxygen atoms to form infinite zigzag chains that run parallel to the *a* axis.

Bond valence sums[24] for all crystallographically unique atoms were calculated and are in good accordance with their formal oxidation states (Table 4). However, O(19), O(20), and O(23) were found to be undersaturated, giving values of 1.28, 1.22, and 1.29, respectively. These low values are typical and indicative of hydrogen bonding and are typical values for O−H bonds within HPO_4^{2-} groups. In addition, O(25) has a calculated valence sum significantly lower at 0.37(2) and is typically associated with the presence of two hydrogen atoms as in the case of water. Although no hydrogen atoms were successfully located within the electron density map around O(25), the magnetic data and thermal analysis leave little doubt that the O(25) is present as a water molecule.

Table 4. Bond Valence Sums for Atoms in $NaBaFe_4(HPO_4)_3(PO_4)_3 \cdot H_2O$

atom	*d*(atom−O)	bond sum[a]	atom	bond sum
Na(1)	2.371−2.700	1.04(4)	O(8)	2.09(5)
Ba(1)	2.727−3.329	2.00(6)	O(9)	2.07(2)
Fe(1)	1.892−2.143	3.17(4)	O(10)	2.01(1)
Fe(2)	1.888−2.121	3.20(5)	O(11)	1.85(2)
Fe(3)	1.925−2.101	2.96(3)	O(12)	1.74(3)
Fe(4)	1.888−2.144	3.17(1)	O(13)	1.91(3)
P(1)	1.516−1.568	4.90(8)	O(14)	1.99(1)
P(2)	1.513−1.567	5.14(4)	O(16)	1.96(1)
P(4)	1.510−1.574	5.07(3)	O(17)	2.05(3)
P(5)	1.493−1.595	5.12(4)	O(18)	2.11(3)
P(6)	1.501−1.546	5.03(4)	O(19)	1.28(2)
O(1)		1.98(4)	O(20)	1.22(1)
O(2)		1.99(3)	O(21)	2.03(1)
O(3)		1.90(3)	O(22)	2.10(4)
O(4)		1.82(3)	O(23)	1.29(3)
O(5)		2.07(2)	O(24)	1.82(3)
O(6)		1.99(3)	O(25)	0.37(2)
O(7)		1.97(1)		

[a] Bond sum $= \exp[r_o - r)/B]$, where r_o = empirically determined parameter from ref 22, $B = 0.37$, and r = bond distance.

Physical Characterization. The TGA for $NaBaFe_4(HPO_4)_3(PO_4)_3 \cdot H_2O$ showed evidence of three weight loss steps consisting of an initial onset at 480 and 580 °C, a broad step between 580 and 620 °C, and another broad step between 620 and 900 °C. The total weight loss corresponds to 4.81%, a value close to the expected 4.6% due to the dehydration of 2.5 mol of water. The nature of the dehydrated product is unknown. The infrared spectrum of $NaBaFe_4(HPO_4)_3(PO_4)_3 \cdot H_2O$ revealed P−O vibrational frequencies[25] associated with the HPO_4^{2-} groups observed as two strong bands centered at 2900 and 2400 cm^{-1} and a broad band of weak intensity centered at 1290 (w−m) cm^{-1}. A split band of strong intensity with peaks centered at 1090 (s) and 990 (s) cm^{-1} due to the PO_4^{3-} groups was also observed. The O−H stretches were present as a broad band centered at 3320 cm^{-1}.

Figure 4 shows the temperature dependence of the magnetic susceptibility and reciprocal susceptibility for $NaBaFe_4(HPO_4)_3(PO_4)_3 \cdot H_2O$. The experimental magnetic moments of the iron sites were calculated from the determined Curie constant (*C*). $NaBaFe_4(HPO_4)_3(PO_4)_3 \cdot H_2O$ displays Curie−Weiss behavior over the temperature range of 48−300 K with a large Weiss constant of $\Theta = 183$ K, which implies that the dominant interactions between neighboring Fe atoms are strong and ferromagnetic, which can be seen by the sharp ferromagnetic transition at the Curie point ($T_c = 8$ K). A Curie constant (*C*) of 19.5 emu K^{-1} per formula unit was derived. A calculated effective magnetic moment/Fe center of $\mu_{eff} = 6.25\ \mu_B$ was determined, which is somewhat higher than expected ideal spin-only value of 5.92 μ_B for a high-spin, $Fe^{3+}(d^5)$ metal in an octahedral environment. This increase is possibly caused by a small angular contribution to the magnetic moment or the presence of imputities.

Ion-Exchange Properties of $NaBaFe_4(HPO_4)_3(PO_4)_3 \cdot H_2O$. Due to the layered structure of this compound, it has the potential for possessing ion-exchange properties as observed

(24) Brown I. D.; Altermatt, D. *Acta Crystallogr.* **1985**, *B41*, 244.

(25) Nyquist, R. A.; Kagel, R. O. *Infrared Spectra of Inorganic Compounds*, 1st ed.; Academic Press: New York, 1971.

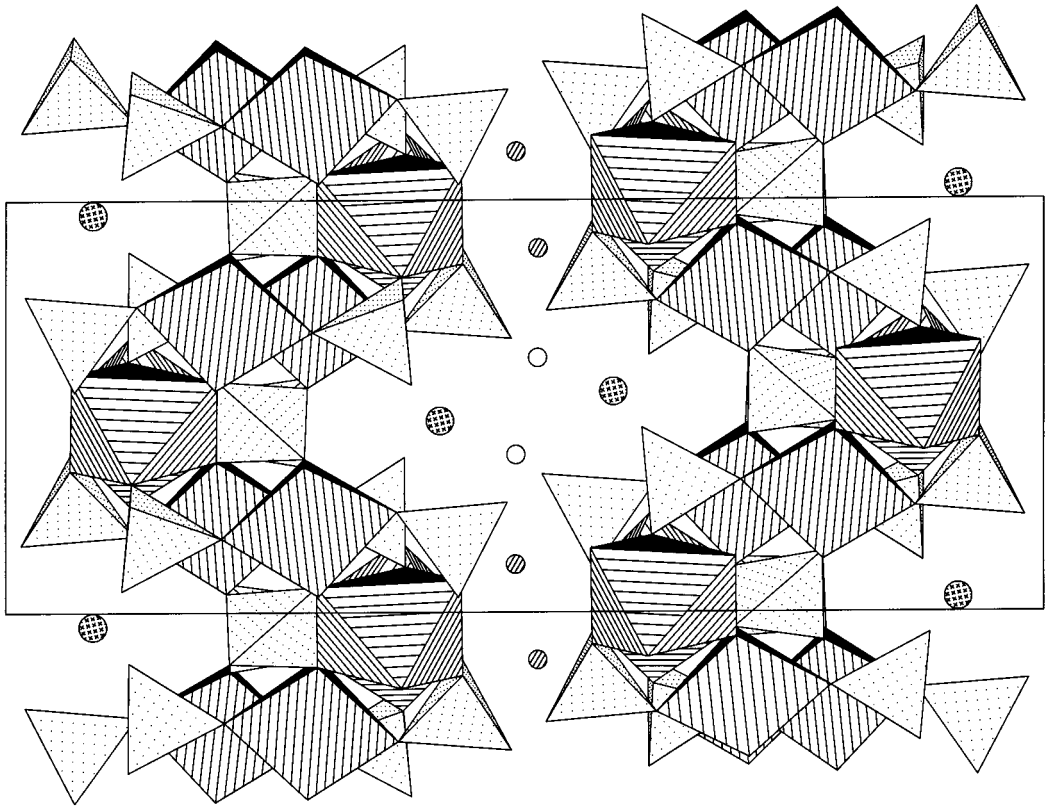

Figure 3. Representation showing how the $P(3)O_4$, $P(4)O_4$, $P(5)O_4$, and $P(6)O_4$ groups link the FeO_6 chains together in the *a* direction and possess a terminal P−O bond that points inward toward the small cavities between the layers.

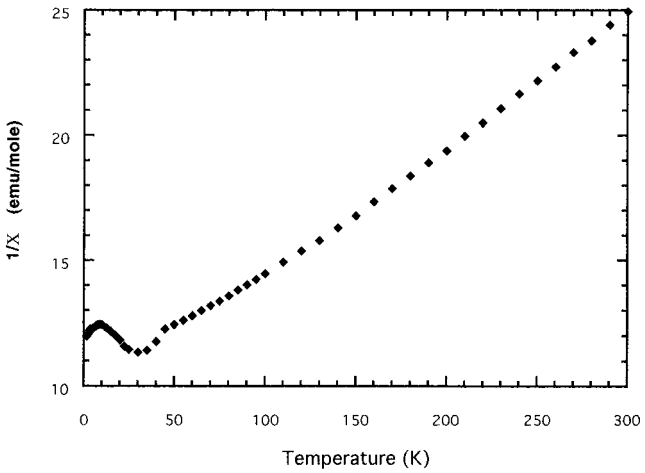

Figure 4. Magnetic susceptibility data for $NaBaFe_4(HPO_4)_3(PO_4)_3 \cdot H_2O$ between 4 and 300 K.

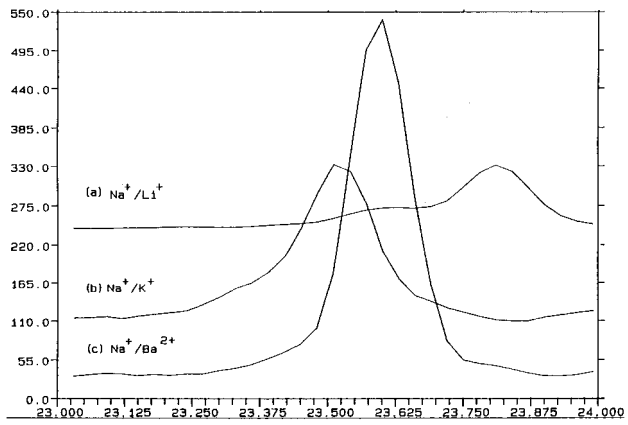

Figure 5. Powder XRD patterns of (a) $Na_{1-x}Li_xBaFe_4(HPO_4)_3(PO_4)_3 \cdot H_2O$, (b) $Na_{1-x}K_xBaFe_4(HPO_4)_3(PO_4)_3 \cdot H_2O$, and (c) $NaBaFe_4(HPO_4)_3(PO_4)_3 \cdot H_2O$, showing the expected shifts in 2θ.

in many natural and synthetic zeolites.[26] Therefore, some simple studies were undertaken to investigate ion exchange of the sodium ion with the remaining alkaline metal cations. Powder XRD of the ion-exchanged samples were run at the same continuous scan speeds as $NaBaFe_4(HPO_4)_3(PO_4)_3 \cdot H_2O$. Figure 5 shows a comparison of the X-ray powder diffraction patterns of both the parent and the ion-exchanged material and suggests a topotactic exchange. Given the *hkl* values from those calculated from the single-crystal data of the parent phase, the lattice parameters of the ion-exchange samples were calculated by refining 35 peaks for each sample. In all cases an appropriate increase or decrease is observed, dependent on the size of the exchange cation, predominately along the *b* axes of the unit cell. For instance, in $NaBaFe_4(HPO_4)_3(PO_4)_3 \cdot H_2O$, the *b* axis is 22.665(4) Å, while, in the exchange products of $Na_{1-x}Li_xBaFe_4(HPO_4)_3(PO_4)_3 \cdot H_2O$ and $Na_{1-x}K_xBaFe_4(HPO_4)_3(PO_4)_3 \cdot H_2O$, the *b* axis is 22.641(3) and 22.685(5) Å, respectively. Table 5 provides all of the lattice parameters for both ion-exchange products as well as the parent phase. Energy-dispersive X-ray analysis of the powdered samples also reveals the presence of the exchanged cation in all cases except lithium, which is below the limits of the detector. However, a significant amount of sodium was still present as well, suggesting that only partial ion exchange occurred. Since attempts to prepare the lithium and potassium end members were unsuccessful, Vegard's law could not be used to determine the percent exchange that occurred. Surprisingly, the rubidium ion exchange proved unsuccessful. The resulting product was not a finely divided powder as are all the others; rather it was very flaky and stuck

(26) Barrer, R. M. *Hydrothermal Chemistry of Zeolites*; Academic Press: London, 1982.

Table 5. Comparison of Lattice Parameters for the Ion-Exchange Compounds of $NaBaFe_4(HPO_4)_3(PO_4)_3 \cdot H_2O$

compound	*a* (Å)	*b* (Å)	*c* (Å)	*V* (Å^3)
$Na_{1-x}Li_xBaFe_4(HPO_4)_3(PO_4)_3 \cdot H_2O$	9.2770(3)	22.641(5)	8.9657(4)	1883.2(6)
$NaBaFe_4(HPO_4)_3(PO_4)_3 \cdot H_2O$	9.2780(2)	22.6651(4)	8.9665(3)	1886.3(8)
$Na_{1-x}K_xBaFe_4(HPO_4)_3(PO_4)_3 \cdot H_2O$	9.2921(5)	22.6855(7)	8.9700(3)	1890.8(5)

to the pestle during grinding. This could possibly be due to the product becoming more hydrated than in the initial sample. Thus the hydrated alkali might be too large to remain within the layered framework. The powder pattern of the Rb^+ exchanged material also revealed that the sample was amorphous. Thus the structure of the solid was destroyed rather than displaying single ion exchange. This might suggest that potassium ion is the largest cation that the compound can accommodate. There is no experimental evidence for Ba^{2+} exchange.

Conclusion

A new layered iron phosphate can be easily prepared in good yield using high-temperature hydrothermal methods. The compound contains edge-shared Fe(III) octahedra built of bridging PO_4^{3-} and HPO_4^{2-} groups with Na^+ and Ba^{2+} cations located between the layers. The compound is valence precise, and the presence of the HPO_4^{2-} groups is confirmed by IR and thermal analysis as well as crystallographic evidence. The magnetic susceptibility indicates that the solid is Curie−Weiss paramagnetic showing a spin only value that suggests high-spin Fe(III). The layered material also undergoes ion exchange under relatively mild conditions, and Li^+ and K^+ are partially exchanged for Na^+. However Rb^+ causes breakup of the lattice, suggesting that possibly the lattice is size limiting. Further investigations to synthesize other phosphates of this type are in progress.

Acknowledgment. We thank the National Science Foundation (Grant CHE-9714408) for financial support for this research and Professor S.-J. Hwu for use of his thermal analysis equipment.

Supporting Information Available: Tables listing detailed crystallographic information along with anisotropic thermal parameters for all atoms and complete bond distances and angles. This material is available free of charge via the Internet at http://pubs.acs.org.

IC0001513